Adjustable Multi-Sector Cellular Base Station Antenna

Senglee Foo, Member, *IEEE*, Bill Vassilakis, Senior Member, *IEEE*

Powerwave Technologies, 1801 E. St. Andrew Place, Santa Ana, CA, 92705
Email: Senglee.Foo@pwav.com, Tel: 714-466-1437

***Abstract* — This article presents a dual beam array (DBA) for higher-order sectorization of a cellular site. This technique provides a means of cost-effective boosting network capacity without the use of additional frequency spectrum. The DBA comprises of a multi-column array and a beam forming circuit, which produces two overlapping beams with adjustable beam patterns. The proposed antenna is an adjustable cylindrical sector array, composed of three separate linear array columns. This structure allows for the formation of two overlapping beams with amplitude and phase excitations which can be implemented using a compact and low loss circuit. The adjustable offset displacement for the center column array allows for the refinement and adjustment of the pattern characteristics of the two overlapping beams. This method results in a beam split loss of less than 0.5dB in comparison to a single beam case. Performance parameters such as the beam cross-over loss and pattern discrimination between beams can also be adjusted in-situ for optimum operation.**

***Index Terms* — Beam forming network, multi-beam, base station antenna, smart antenna, multi-sector array.**

I. INTRODUCTION

Higher order sectorization provides a means of increasing cellular network capacity and providing optimum coverage without the use of additional frequency spectrum. Partial use of higher order sectorization is particularly useful for cost-effective accommodation of service growth in a localized service area within a cellular coverage. In these localized 'hotspot' areas antennas with multiple beams of narrower beamwidth and higher directivity can be used to increase the overall capacity. For instance, one of the 65 degree sectors within a cell site that has a higher traffic may be served using two overlapping beams of 33 degrees. This method allows an increase in an overall network capacity by using multiple columns of linear array arranged on a cylindrical curvature. This arrangement results in an amplitude and phase excitation that can be implemented using a simple and low-loss beam-forming network. It produces two symmetrical beams with respect to the azimuth boresight. Radiation patterns of the two beams are overlapped in the manner that the coverage of the cellular sector can be optimized using the adjustable beam array.

Multibeam patterns of a multi-column array are typically formed using a combination of hybrids, couplers and phase shifters [2-4]. This general beam forming method often incurs an additional front-end loss as a result of circuit path losses and signal split between beams. Furthermore, a general beam forming method often requires multiple crossing between input feed lines, which can cause difficulties in the actual beam-forming circuit implementation. This article is an extension of the previous reports [1][5], which presents the concept and test results of a proposed dual beam array (DBA) and the associated beam forming structure for use in efficient beam forming of two overlapping beams. Details of simulations and test results are also included. The adjustable DBA and the associated BFN technology under this development are patent pending and are strictly proprietary to Powerwave Technologies.

A brief summary of the concept, design goals, and critical parameters of the proposed DBA is given in Section II. Section III describes theoretical background and feasibility of the implementation using a three-column array, while the proposed concept and implementation of the compact 3-to-2 microstrip beam forming network is given in Section IV. The geometry and performances of the broad beamwidth aperture-coupled patch is described in Section V. EM Simulations using HFSS and measured radiations patterns using spherical near-field range is given in Section VI and Section VII, respectively. Section VIII briefly compares and discusses the theoretical and measured results. Section IX concludes the paper.

II. DUAL BEAM ARRAY

Fig. 1 shows the concept of the proposed dual beam array. Each of the overlapping beams has a typical HPBW of 33 deg. The design is such that the combined pattern of the array matches the required coverage of a typical cellular sector (65 degree coverage). The dual beam array can potentially increase the overall capacity because of the narrower beams and higher antenna directivities. However, because the two beams are adjacent to each other, compromises in antenna performances such as signal interference between the two beams and hand-over loss are often required. By using a three-column array with a movable center column, these compromises can be made adjustable in-situ to meet any particular need.

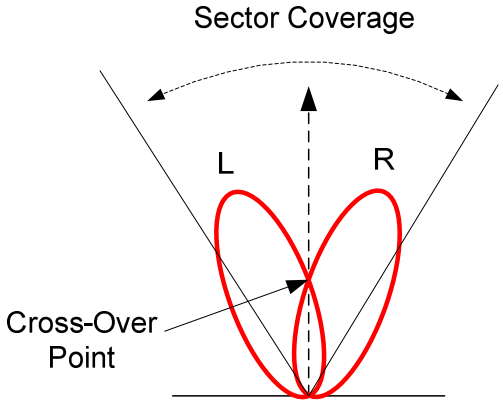

Fig.1. Dual beam concept

Fig. 2 shows a schematic of the 3x2 beam forming network (BFN). Two simultaneous beams are formed using three separate columns of linear array, which consists of a number of dual polarized aperture-couple patches (ACP).

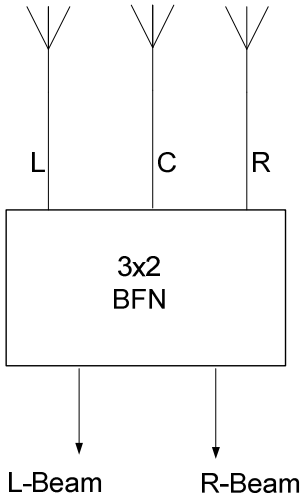

Fig. 2. Three-column dual beam BFN

Table 1 gives a summary of the desired antenna parameters of the DBA. In this case, the antenna is designed for UMTS band, 1700MHz to 2200MHz. The total coverage angle is typically 67 degree. Beamwidth of the dual beams is expected to be approximately 33 degree.

Key parameters of the dual-beam array are: (1) Aperture size and overall RF beam forming losses, (2) signal interference between the two adjacent beams, (3) loss factor at the cross-over (hand-over) point. A typical DBA using conventional beam forming technique cannot deliver optimum performance in all these aspects.

Table 1: Antenna Parameters

	Parameter	
1	Frequency	1710 - 2150 MHz
2	Az Beamwidth	Individual : 33 to 45 deg
		Combined : 67 to 92 deg
3	El Beamwidth	6 - 8 deg
4	Directivity	19.7 to 21.3 dBi
5	Polarization	±45 deg
6	El Tilt	6-7 deg (RET)
7	Cross-pol Level	< -20dB
8	Cross-over loss	2.5 dB to 6.5 dB
9	Upper SLL	-18 dB (relative to main beam, 30 deg above horizon)
10	Port-port Isolation	30 dB
11	F/B	30 dB
12	Return Loss	-14 dB
13	Power Handling	200W (CW)
14	Passive Intermod	-150 dBc (3rd order)
15	Mechanical	
	Length	1.4m
	Width	28cm
	Depth	15cm

The goal of this study is to develop a DBA which will permit trade-off and compromises between these parameters in order to achieve the optimum performance for a given application. The design will allow trade-off between signal interference and the cross-over loss between the two beams.

III. 3-COLUMN DUAL BEAM ARRAY

The proposed antenna can be perceived as a superposition of two partially-filled ring arrays. The azimuth pattern of the two-ring circular array can be varied by adjusting the relative dimension of the radiuses of the rings. Fig. 3 depicts the theoretical model of a general two-ring array.

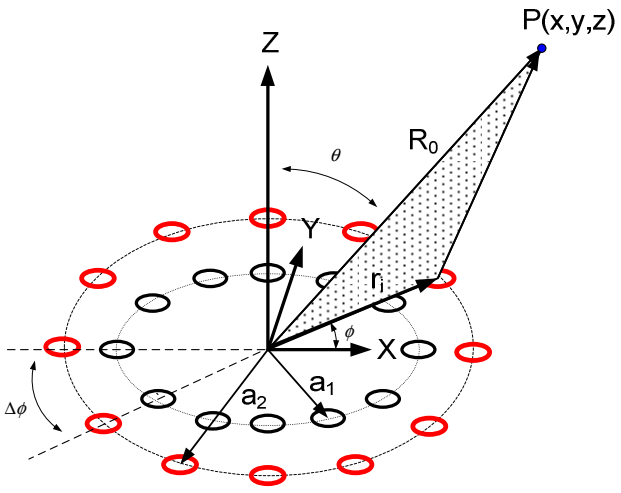

Fig.3. Theoretical two-ring concept of the dual beam array

A simplified mathematical model for the total field of the three-column two-ring array is

$$\hat{F}(\theta,\phi) = I_1 * \hat{E}_1(\theta,\phi) * \exp[\,jka_1 \sin\theta\cos(\phi-\Delta\phi)] + I_0 * \hat{E}_0(\theta,\phi) * \exp[\,jka_2 \sin\theta\cos(\phi)] + I_{-1} * \hat{E}_{-1}(\theta,\phi) * \exp[\,jka_1 \sin\theta\cos(\phi+\Delta\phi)] \quad (1)$$

Where,

$$\hat{E}_1(\theta,\phi) = \hat{E}_0(\theta,\phi-\Delta\phi) \quad (2)$$

$$\hat{E}_{-1}(\theta,\phi) = \hat{E}_0(\theta,\phi+\Delta\phi) \quad (3)$$

$\hat{E}_0(\theta,\phi)$ represents element pattern of radiators on the center column. I_1 and I_{-1} are complex coefficients of excitations for radiators 1 and -1. Radiuses of the two rings are a_1 and a_2, respectively. k is the wave number. $\Delta\phi$ is the angular spacing between radiating elements.

Fig. 4 shows the front and cross-sectional views of the 30-element, three-column, cylindrical sector array. The array is designed to operate in a typical wireless communication band, 1700 MHz to 2200 MHz.

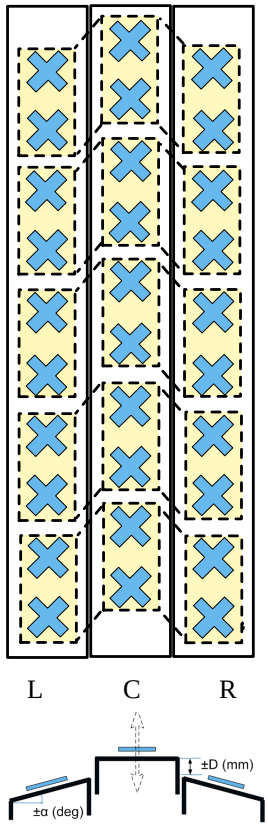

Fig. 4. Three-column array with adjustable center column

The radiating elements are aperture-coupled patches. Each of the three linear arrays is mounted on a separate reflector. Radius of the inside ring, a_1, is determined by the subtend angle of the two edge reflectors, **α**. Radius of the outside ring, a_2, is set and adjusted by the vertical displacement, D, which can be varied between -5mm to +25mm in the direction of the mechanical boresight direction.

The relative slope of the two edge columns, α, with respect to the center column, is critical in achieving the required pattern shapes and beam cross-over loss. Typically, this angle is set between 20 degree and 30 degree with respect to the center column. With these parameters, the dual beam patterns can be maintained over a relatively broad frequency bandwidth. Fig. 5 shows a simulated 65˚ full coverage beam pattern and three independent narrow beams at 2200 MHz. For these analyses, the angle (α) is set at 20 degree. The half-power-beamwidth (HPBW) of each individual narrow beam is approximately 33 degree, which provides combined azimuth coverage of 65 degree for a typical cell sector.

For some applications, it is possible that signals are transmitted at one polarization using the broad beam pattern (65 degree), while the receive signals at other polarization using the two narrow beams. For other applications, both transmit and receive signals operate using the dual beams. A narrow center beam can also be formed if necessary. Combinations of these can be formed depending on the application.

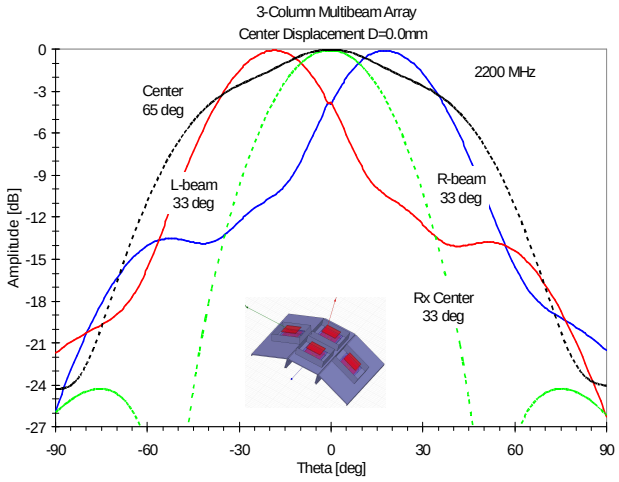

Fig. 5. Simulated beam patterns of the three-column array

With the displacement distance of the center column set at D=0mm (reflector surface of the center column levels with the top edges of the two edge columns), the three narrow beams and the 65˚ broad beam pattern can be formed using the amplitude and phase excitations given in Table 2.

Table 2. Amplitude and Phase excitations for various beams

Beam	Left (L)	Center (C)	Right (R)
Left 33˚	(1, 0˚+Δφ)	(0.74, 0˚)	(0.34,-180˚+Δφ)
Center 33˚	(0.5, 0˚+Δφ)	(1.0, -30˚)	(0.5, 0˚+Δφ)
Right 33˚	(0.34,-180˚+Δφ)	(0.74, 0˚)	(1.0, 0˚+Δφ)
65˚ Beam	(0.5, -45˚)	(1.0, 0˚)	(0.5, -45˚)

Δφ represents an additional phase adjustment, which can be introduced into the excitation by the addition of a fixed line length on the feed line, or varying the relative displacement distance of the center column, D. This adjustable phase allows further optimization of beam parameters such as the beam cross-over losses and pattern discrimination.

IV. BEAM FORMING CIRCUIT

Fig. 6 shows the amplitude and phase excitations of the 3-to-2 beam forming network for the dual beam patterns. Fig. 7 and 8 show the equivalent signal diagram and the implementation of the compact dual beam former using micorstrip transmission line method.

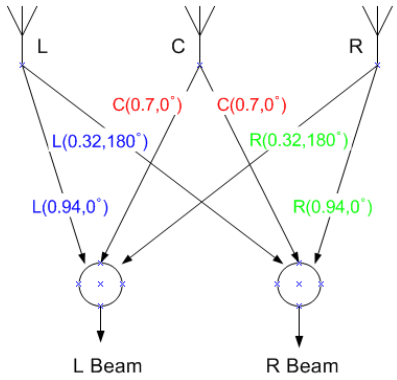

Fig. 6. Excitations function of the dual beam former

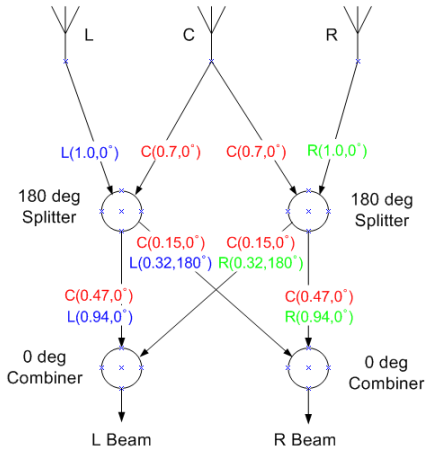

Fig. 7. Equivalent excitation signal diagram of the dual beam former

The proposed 3-to-2 beam former is implemented using two unequally-split 180deg splitters and two in-phase Wilkinson combiners. This simple implementation has an added advantage of excellent isolations between antenna ports as shown in Fig. 9, simulated using Agilent ADS. These are inherent merits from port cancellation at the sum and difference ports of the 180 degree splitters.

Another significant advantage of this implementation is the low beam-split signal losses. Each of the dual beams are formed using a 180 degree splitter (10 dB) on the corresponding edge column and a 3dB (0 deg) splitter on the center column. The total signal loss due to the beam split is less than 0.5 dB in comparison to the single beam case (center 33˚), which has an excitation taper of (0.5, 1.0, 0.5). This is a direct result of the optimum phase and amplitude tapers from the array configuration. Furthermore, the path loss is also minimized because of the compact circuit design.

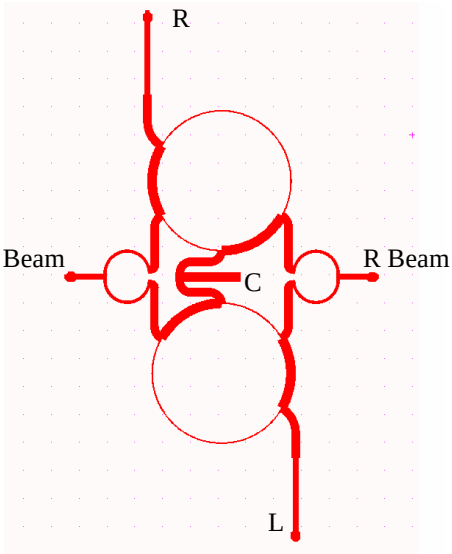

Fig. 8. Microstrip implementation of the compact dual beam former

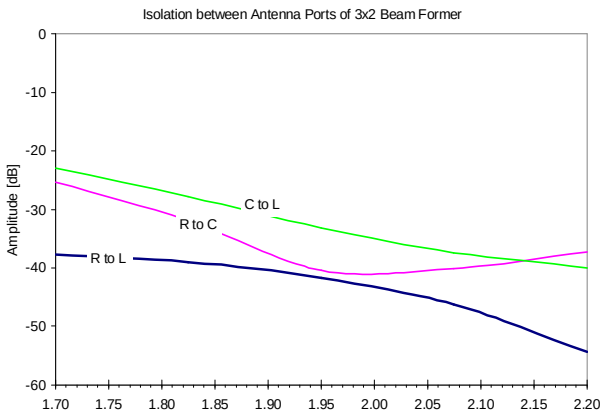

Fig. 9. Isolation between antenna ports of dual beam former

V. APERTURE-COUPLED PATCH (ACP)

One of the critical elements of this development is the dual-polarized radiators with relatively broad beamwidth over a large operating frequency. For optimum array performance, it is desirable that the azimuth pattern of the radiator can be adjusted to allow optimization of the azimuth beam pattern, port isolations, and the overall directivity of the array.

Use of metallic boundaries in the near-field enables broadening of HPBW of a patch antenna up to approximately 90 deg at the expense of the overall frequency bandwidth. The proposed method of dielectric fortification [5] between the radiator and the metallic boundaries provides a systematic means for significant broadening of HPBW over a large frequency bandwidth. Subsequently, this method allows optimization of array performance by selecting appropriate thickness or height of the dielectric material. The dielectric loading in this manner does not seem to degrade performance in the cross polarization pattern as long as the dielectric loading is symmetrical in all four directions.

Fig. 10 shows the isometric and cross-sectional views of a dielectric fortified stacked patch. In this case, the aperture-coupled stacked patch is dual linearly polarized. Two radiating patches are fed by a pair of orthogonal cross slots on the bottom ground. The radiating patches are centered in a square area with a perimeter formed by four dielectric walls with the outside dimension of approximately half-wave length. The outside surfaces of the dielectric walls can be backed by electrically conductive walls. This arrangement allows a compact construction of the patches. The top radiating patch can be conveniently flash-mounted on top of the dielectric walls, while the lower radiating patch are secured at a predetermined height from the ground via small recessed grooves cut onto the inside surfaces of the dielectric walls.

The electrically conductive layer may be of the equal height as the dielectric walls, or preferably recessed from the top of the dielectric walls for better frequency bandwidth. For a given dielectric material with a fixed height, the HPBW is directly proportional to the thickness of the dielectric walls.

A fullwave FEM model of a dual-polarized aperture-coupled stacked patch with dielectric fortification is simulated using the Ansoft HFSS. For the purposes of these demonstrations, FR-4 (ε_r=4.6) is assumed for dielectric material. The height of dielectric walls is fixed at 20mm and the height of the metallic boundaries is kept at 14mm. Fig. 11 shows the simulated azimuth HPBW for various thicknesses of dielectric walls. As indicated in the figure, the HPBW is varying from 70 degree to 125 degree for value of the dielectric thickness between 0 mm and 7.5mm.

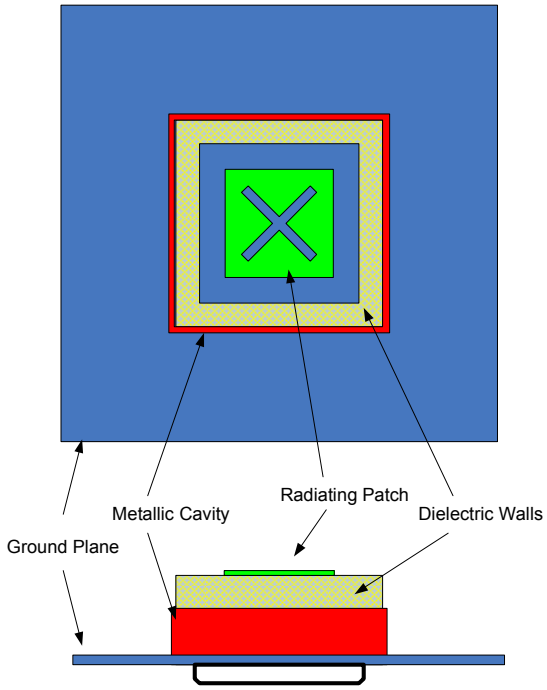

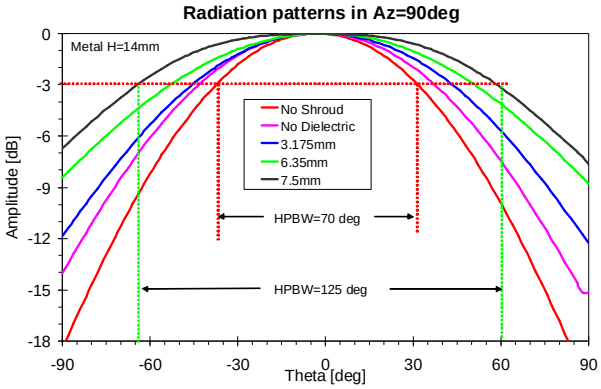

Fig. 11: HPBW of the dielectric fortified stacked patch

VI. EM SIMULATIONS

A 4-element sub-array model of the three-column array is simulated using the Ansoft 3D full-wave Finite Element Method (FEM) HFSS. For these analyses, the subtend angle is set to 20 degree. Fig. 12 and 13 show the simulated azimuth patterns at 1700 MHz and 2200 MHz with the displacement distance (D) set at 0mm.

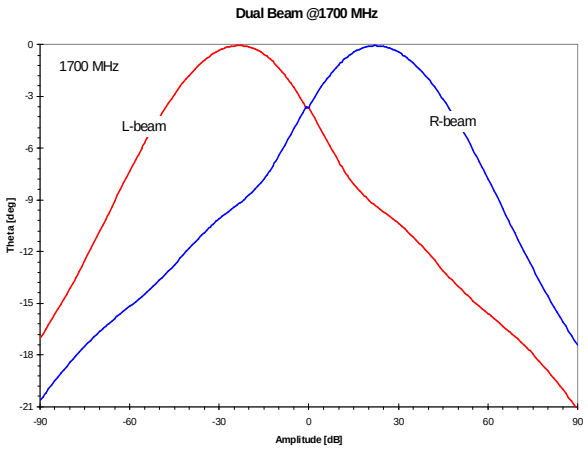

Fig. 12. Simulated dual beam patterns at 1700 MHz

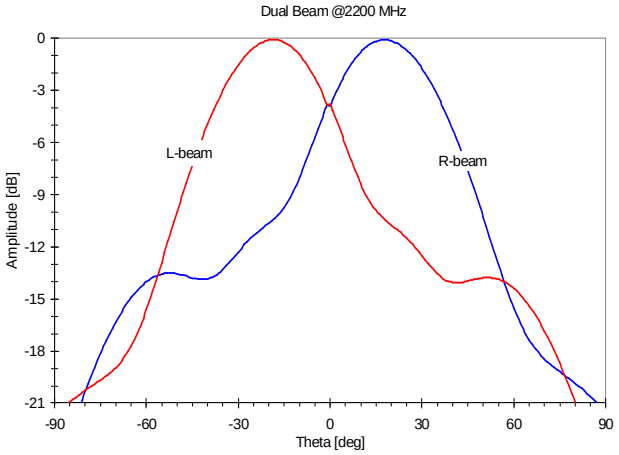

Fig. 13. Simulated dual beam patterns at 2200 MHz

At this setting, the beam cross-over loss at azimuth=0 deg is between 3.5dB@1700 MHz to 3.7dB@2200 MHz (D =0mm). These beam patterns and the cross-over losses can be varied by introducing an additional phase offset between the center column and the two edge columns using the adjustable displacement feature of the array. Fig 14 shows comparisons of the dual beam patterns for the displacement distance at various positions: -5mm, 0mm, and +15mm.

When displacement distance (D) is between -5mm and +15mm, the beam cross-over loss is varying between -1.6dB to -4.9 dB. The lowest beam cross-over loss is -1.6 dB when the displacement distance is at D=-10mm. This low cross-over loss, however, comes at the expense of pattern discrimination performance (4dB at beam peak).

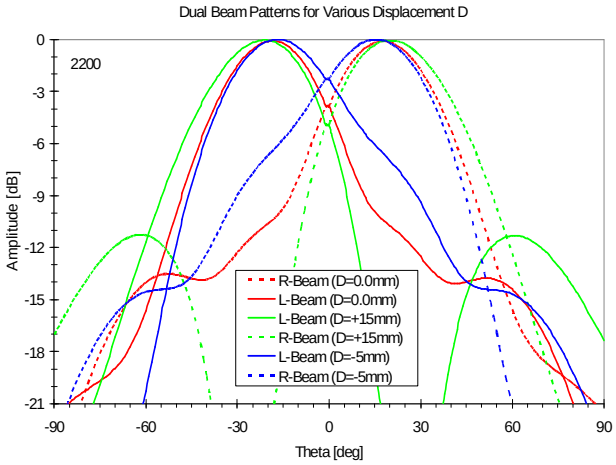

Fig. 14. Dual beam patterns for various displacement distance D

On the other hand, at D=+15mm, the dual beams has an optimum pattern discrimination of over 24dB at the expense of the beam cross-over loss of -4.9dB. Table 3 summarizes the dual beam performances for various displacement distance D.

Table 3. Pattern parameters at various displacement distance D

Displacement Distance	Cross-over Loss	Discrimination At Peak	HPBW (deg)
D=-10 mm	-1.6 dB	4 dB	36
D=-5.0mm	-2.3 dB	6.5 dB	35
D= 0.0mm	-3.7 dB	10.5 dB	33
D=+15mm	-4.9 dB	24 dB	35

These results clearly demonstrated the advantage of the variable displacement of the center column, which allows optimization of performance between hand-over loss (cross-over loss) and interference discrimination.

VII. Measured Results

Fig. 15 show the prototype of the dual-beam array constructed based on the principle of the three-column variable beamwidth array presented in the previous sections. A total of five 3x2 microstrip BFNs are used to feed the 30-element array. Two 1-to-5 elevation power combiner & phase shifter (RET) are used to distribute the BFN Outputs of the left (L) and right (R) beams. This allows separate beam tilt of the R and the L beams in elevation plane between 0 and 7 degree.

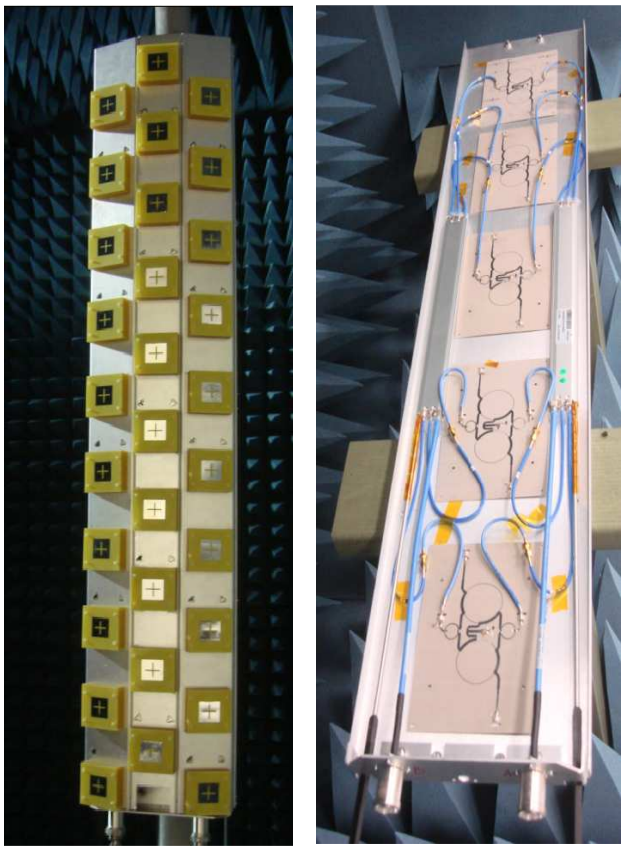

Fig.15.Prototype of the 3-Column DBA and BFN Feeds

Fig. 16 shows the detailed layout of the 3x2 BFN circuit. Outputs of the three linear arrays (Left, Center, Right) are fed to the BFNs at L, C and R, respectively. The Wilkinson combiners produce the Right and Left beams as indicated.

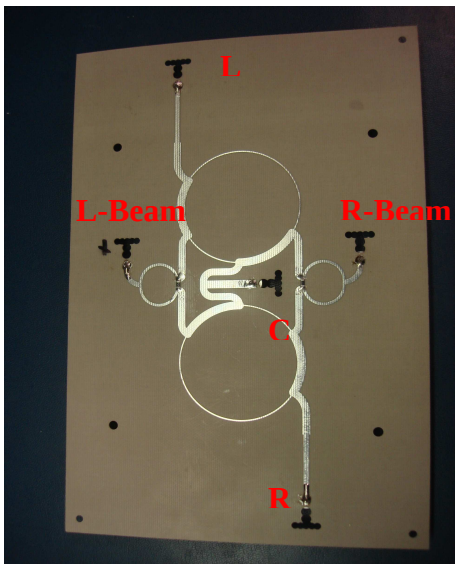

Fig.16. 3-Column Dual Beam Array and BFN Feeds

Table 4 gives the measured amplitudes and phases of the BFN.

Table 4: Measured BFN excitation functions

	1700 MHz		2200 MHz	
R-Beam	Amp	Phase	Amp	Phase
Center	0.96	0.0	0.92	0.0
Right	1.0	- 37.0	1.0	-45.0
Left	0.44	-200.0	0.376	-223.0
L-Beam				
Center	0.96	0.0	0.92	0.0
Right	0.44	-200.0	0.376	-223.0
Left	1.0	-37.0	1.0	-45.0

Antenna patterns of the array were measured in the Powerwave spherical near-field chamber in Santa Ana, California. Two polarizations (slant ±45deg) are measured at two RET settings (0 deg tilt and 7 deg tilt).

Fig. 17 shows the measured azimuth beam patterns (1710MHz, 1950MHz, 2150 MHz) of the DBA when the RET is set to 0 deg and center displacement D=-10mm. At this setting, the measured HPBW is between 32deg to 39deg with cross-over loss between -3.5dB to -3.9dB. The array produces very low cross-polar field components at well below -20 dB. Fig. 18 shows the measured azimuth beam patterns of the DBA when the RET remains set at 0 deg but the center displacement D is moved to -5mm. The HPBW is reduced very slightly, but the cross-over loss is increased to between -4.0dB to -4.4dB. Fig. 19 gives the measured patterns when the displacement is set to 0mm. The HPBW is reduced to between 31 deg and 37 deg, while the cross-over loss is approximately -4.9dB for all frequencies. As shown in Fig. 20, as the displacement is moved up to +10mm, the HPBW is increased to over 36deg and the cross over loss is over 5.9dB.

Fig. 21 to 23 show the azimuth patterns of the DBA when the RET is set to 7 deg. These results are similar to the previous when RET is set to 0deg. However, the cross-over losses are generally lower. For instance, the cross-over loss is reduced to -2.3 dB when the displacement D=-10mm. This is significantly lower than the previous case. However, this comes at the price of lower beam discrimination.

Fig. 24 gives the measured elevation patterns of the array at 1710MHz and 2150MHz when RET=0deg, for various displacement D. Similarly, Fig. 23 gives the elevation patterns for RET=7deg. Apparently, the offset distance (D) does not seem to affect the beam patterns in the elevation plane significantly. However, SLLs tend to increase as the offset distance decreases.

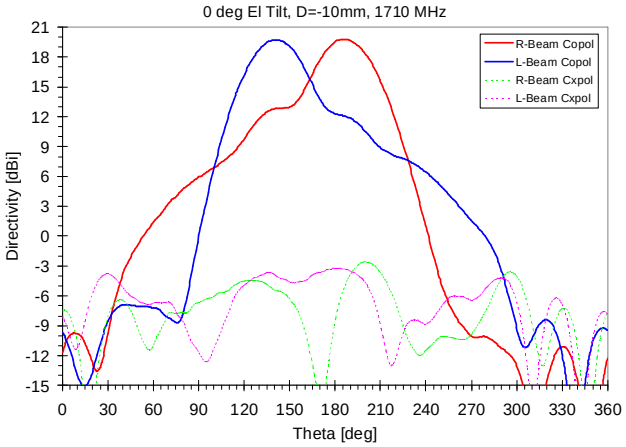

Fig.17(a) Measured DBA Az Pattern (0deg Tilt, D=-10mm, 1710MHz)

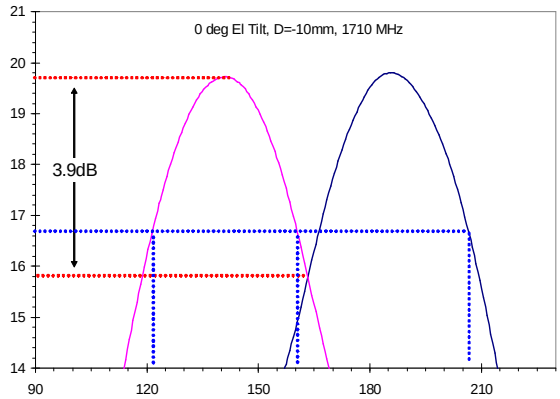

Fig.17(b) Measured cross-over loss (0deg Tilt, D=-10mm, 1710MHz)

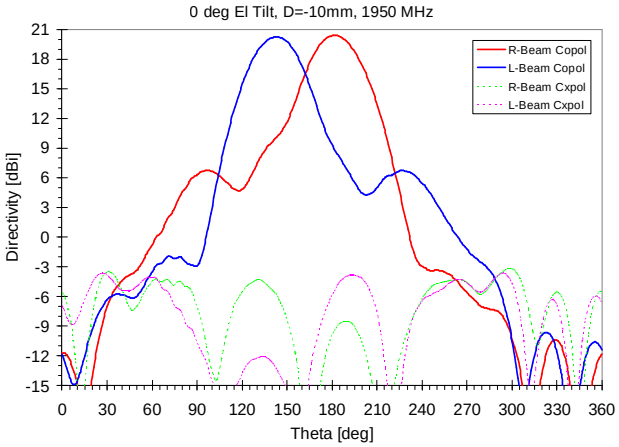

Fig.17(c) Measured DBA Az Pattern (0deg Tilt, D=-10mm, 1950MHz)

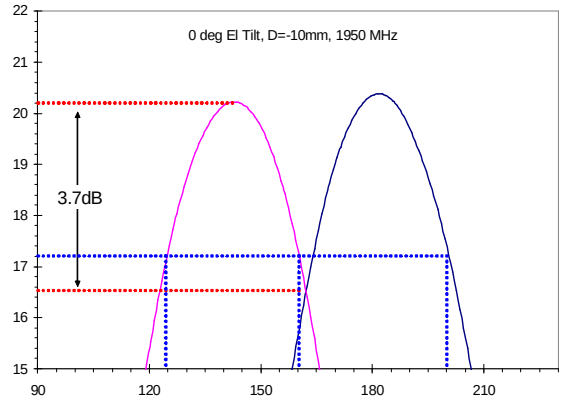

Fig.17(d) Measured cross-over loss (0deg Tilt, D=-10mm, 1950MHz)

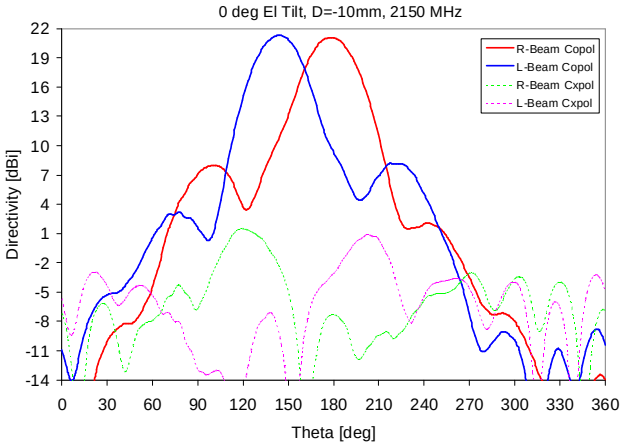

Fig.17(e) Measured DBA Az Pattern (0deg Tilt, D=-10mm, 2200MHz)

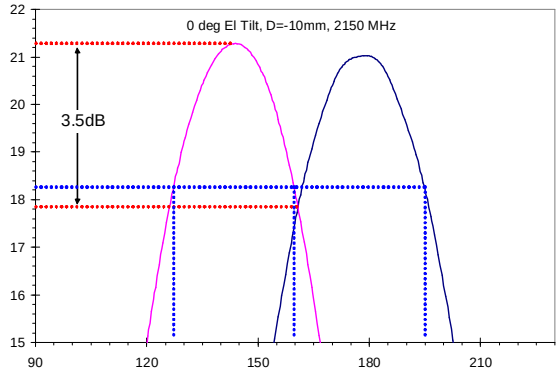

Fig.17(f) Measured cross-over loss (0deg Tilt, D=-10mm, 2200MHz)

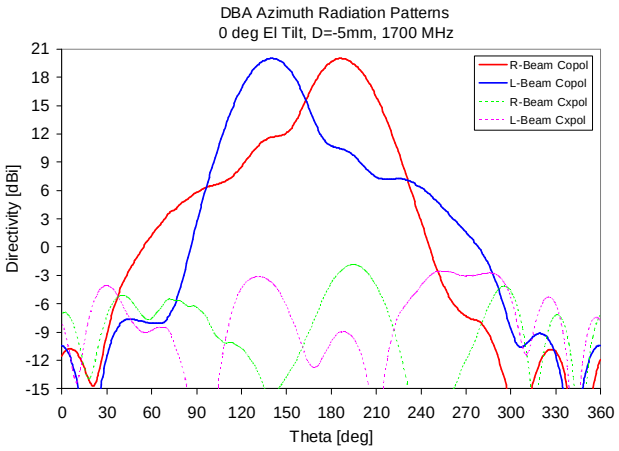

Fig.18(a) Measured DBA Az Pattern (0deg Tilt, D=-5mm, 1710MHz)

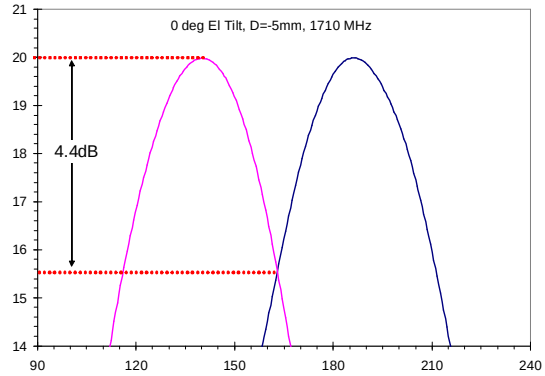

Fig.18(b) Measured cross-over loss (0deg Tilt, D=-5mm, 1710MHz)

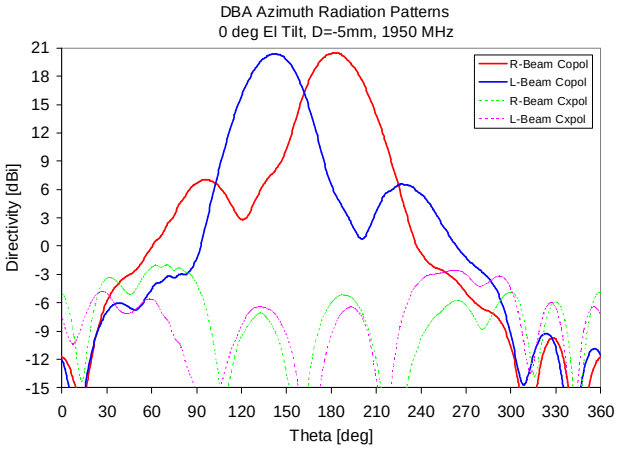

Fig.18(c) Measured DBA Az Pattern (0deg Tilt, D=-5mm, 1950MHz)

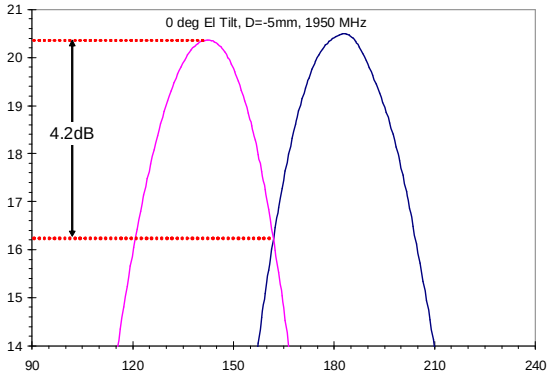

Fig.18(d) Measured cross-over loss (0deg Tilt, D=-5mm, 1950MHz)

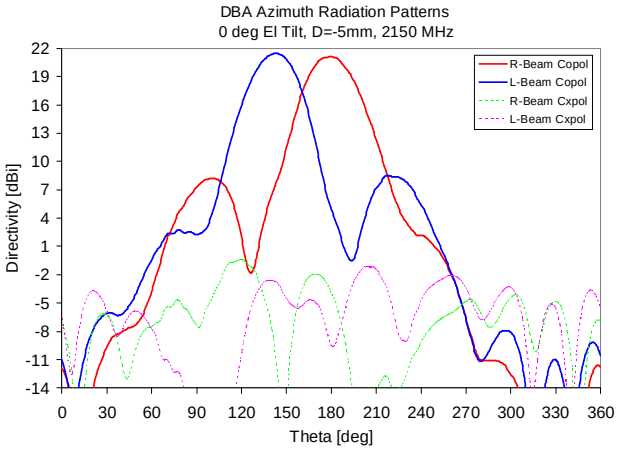

Fig.18(e) Measured DBA Az Pattern (0deg Tilt, D=-5mm, 2200MHz)

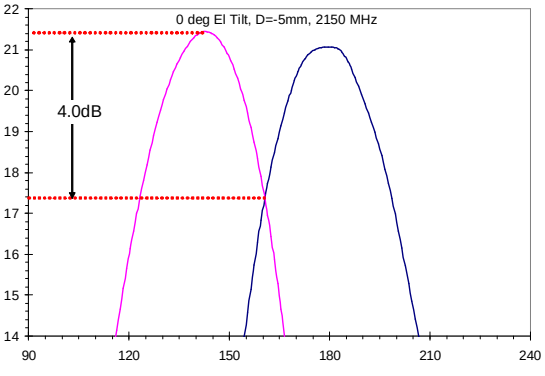

Fig.18(f) Measured cross-over loss (0deg Tilt, D=-5mm, 2200MHz)

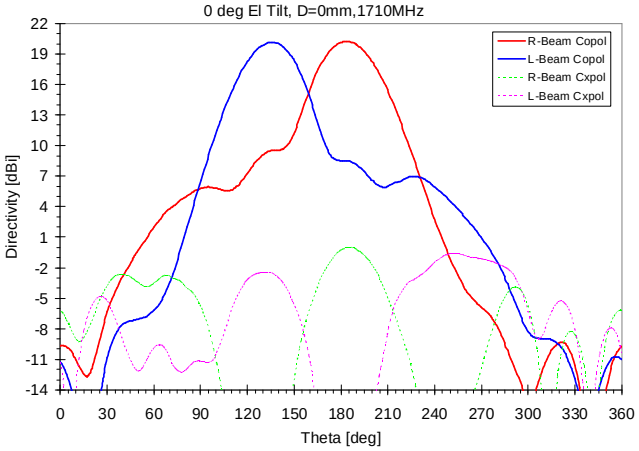

Fig.19(a) Measured DBA Az Pattern (0deg Tilt, D=0mm, 1710MHz)

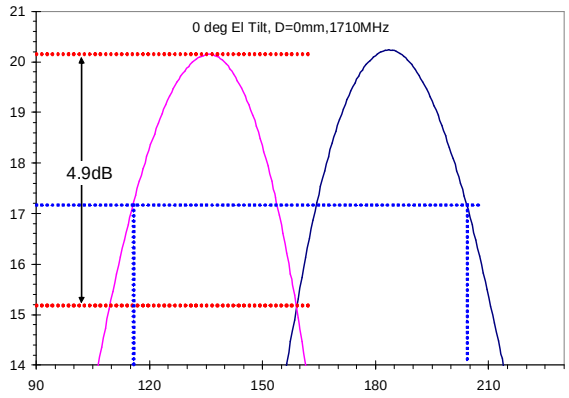

Fig.19(b) Measured cross-over loss (0deg Tilt, D=0mm, 1710MHz)

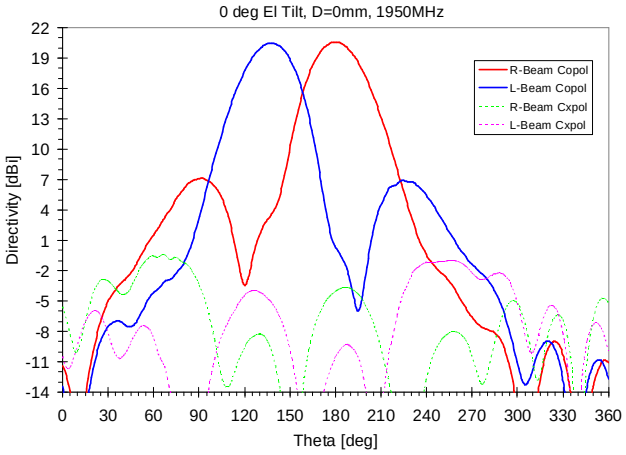

Fig.19(c) Measured DBA Az Pattern (0deg Tilt, D=0mm, 1950MHz)

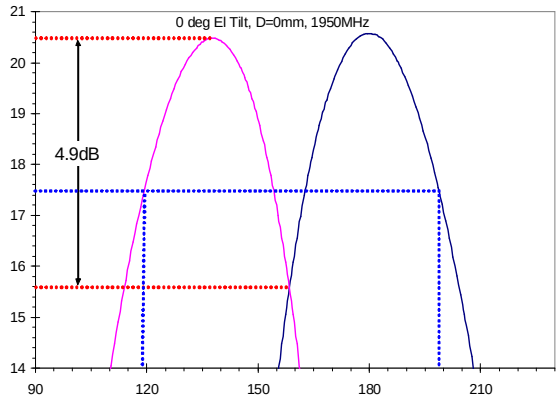

Fig.19(d) Measured cross-over loss (0deg Tilt, D=0mm, 1950MHz)

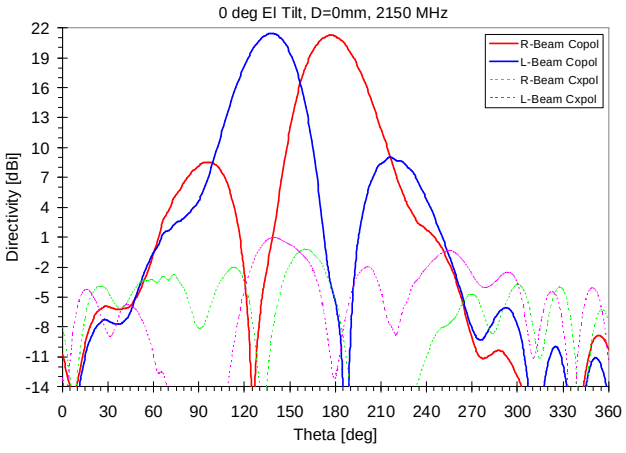

Fig.19(e) Measured DBA Az Pattern (0deg Tilt, D=0mm, 2200MHz)

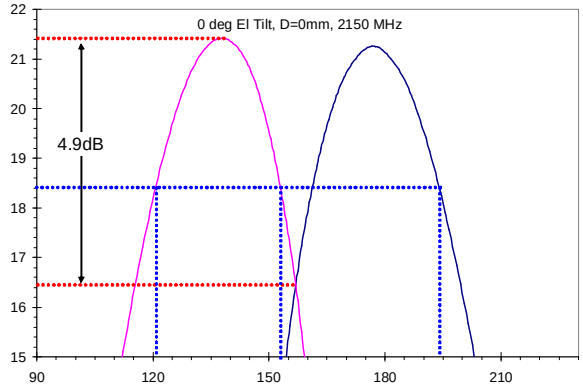

Fig.19(f) Measured cross-over loss (0deg Tilt, D=0mm, 2200MHz)

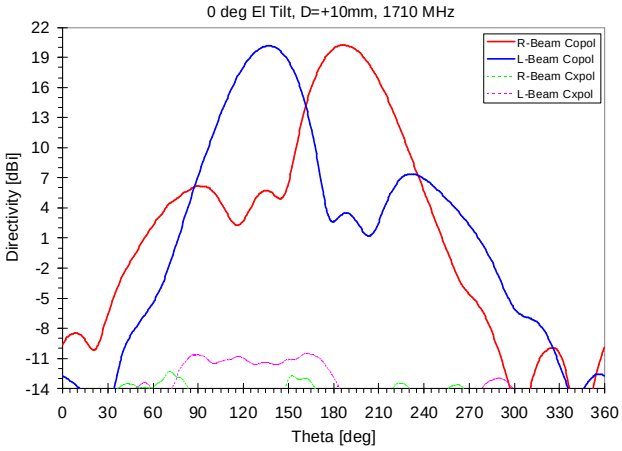

Fig.20(a) Measured DBA Az Pattern (0deg Tilt, D=+10mm, 1710MHz)

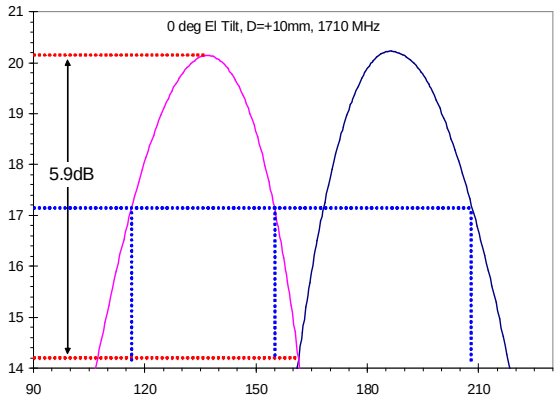

Fig.20(b) Measured cross-over loss (0deg Tilt, D=+10mm, 1710MHz)

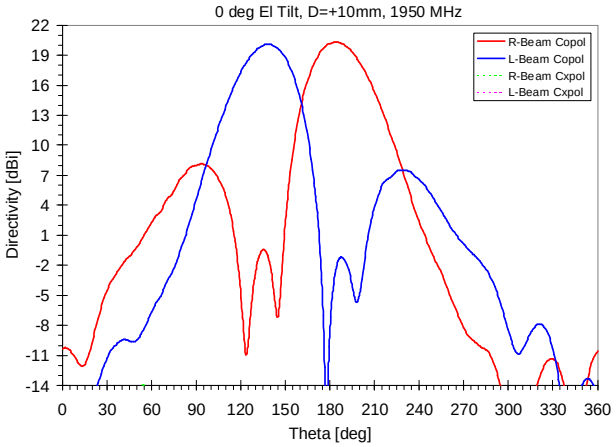

Fig.20(c) Measured DBA Az Pattern (0deg Tilt, D=+10mm, 1950MHz)

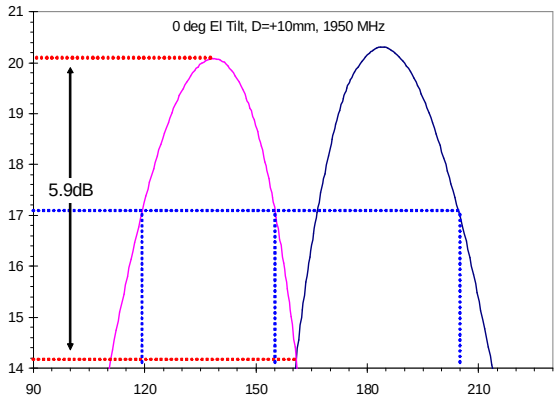

Fig.20(d) Measured cross-over loss (0deg Tilt, D=+10mm, 1950MHz)

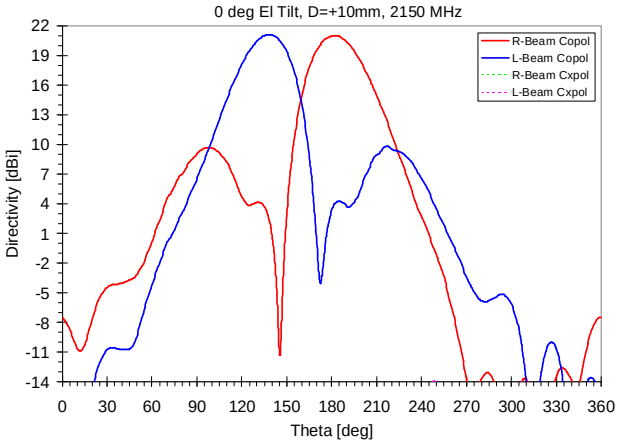

Fig.20(e) Measured DBA Az Pattern (0deg Tilt, D=+10mm, 2200MHz)

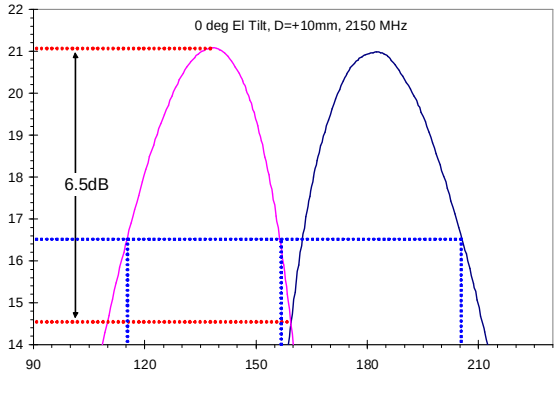

Fig.20(f) Measured cross-over loss (0deg Tilt, D=+10mm, 2200MHz)

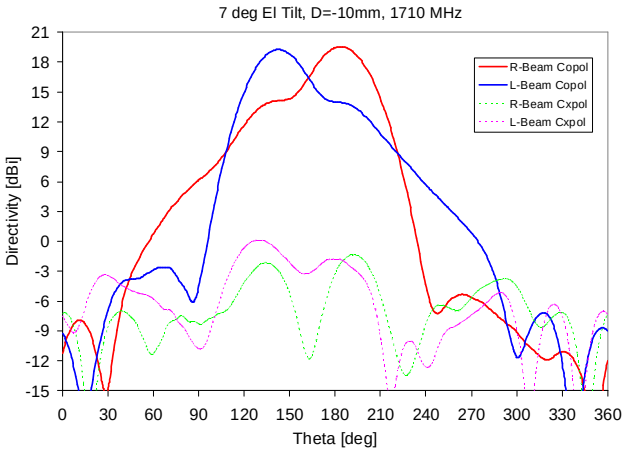

Fig.21(a) Measured DBA Az Pattern (7deg Tilt, D=-10mm, 1710MHz)

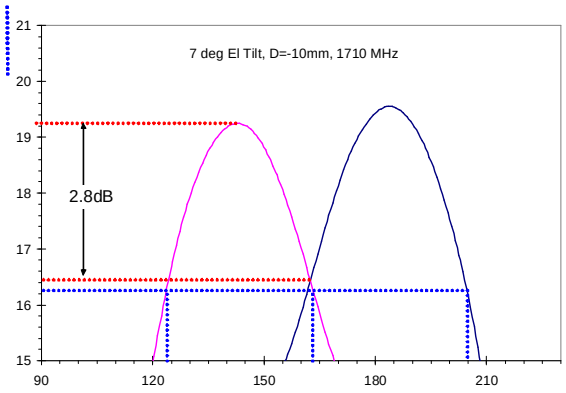

Fig.21(b) Measured cross-over loss (7deg Tilt, D=-10mm, 1710MHz)

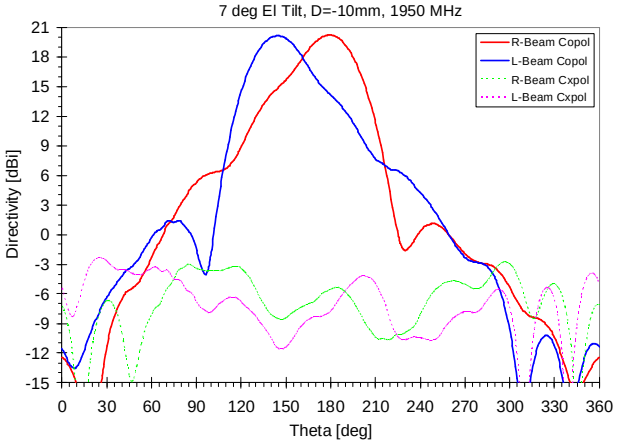

Fig.21(c) Measured DBA Az Pattern (7deg Tilt, D=-10mm, 1950MHz)

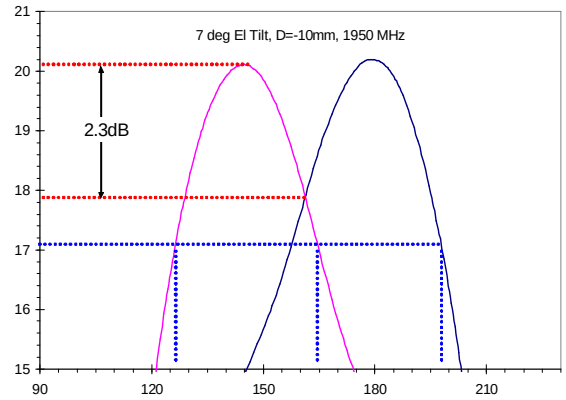

Fig.21(d) Measured cross-over loss (7deg Tilt, D=-10mm, 1950MHz)

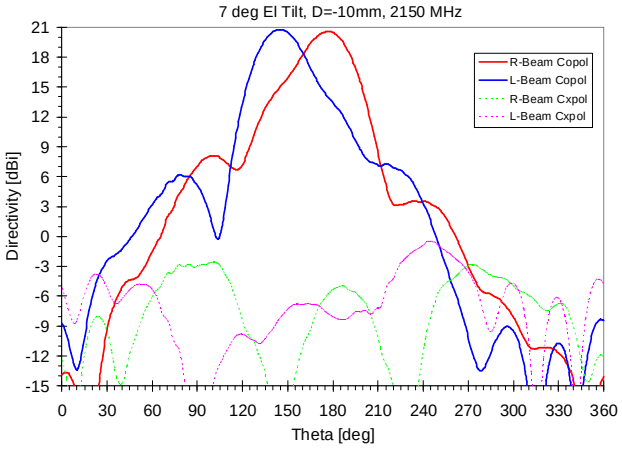

Fig.21(e) Measured DBA Az Pattern (7deg Tilt, D=-10mm, 2200MHz)

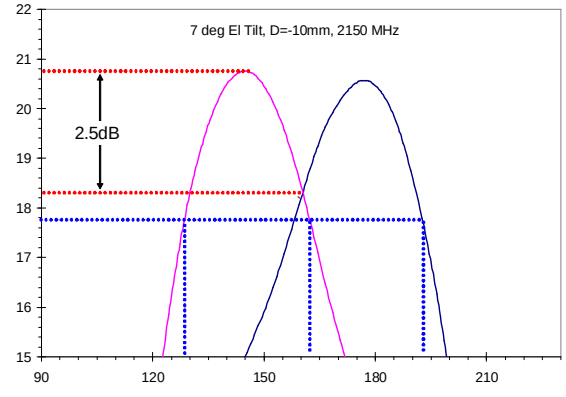

Fig.21(f) Measured cross-over loss (7deg Tilt, D=-10mm, 2200MHz)

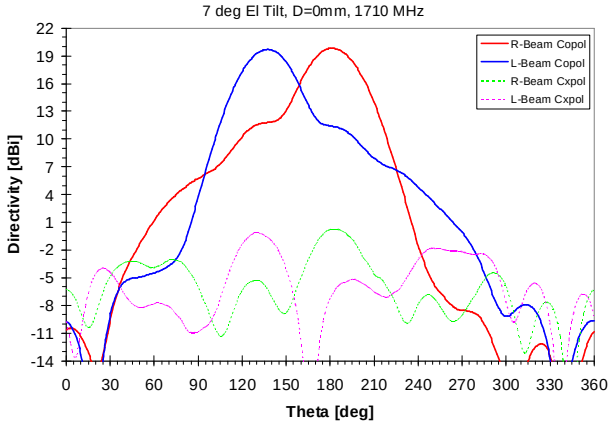

Fig.22(a) Measured DBA Az Pattern (7deg Tilt, D=0mm, 1710MHz)

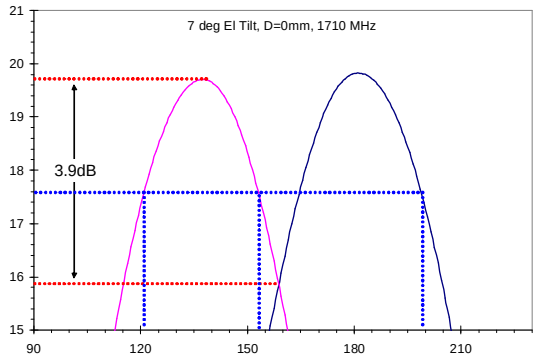

Fig.22(b) Measured cross-over loss (7deg Tilt, D=0mm, 1710MHz)

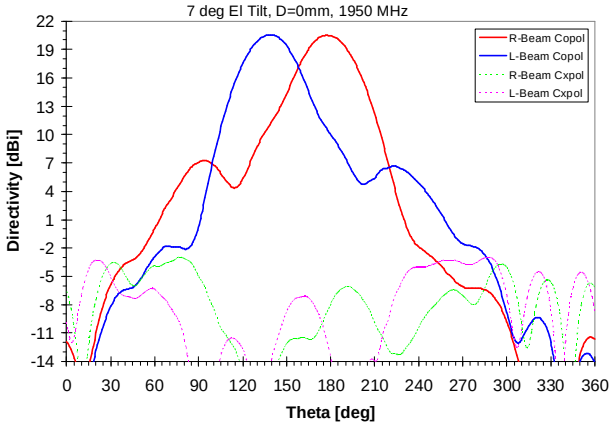

Fig.22(c) Measured DBA Az Pattern (7deg Tilt, D=0mm, 1950MHz)

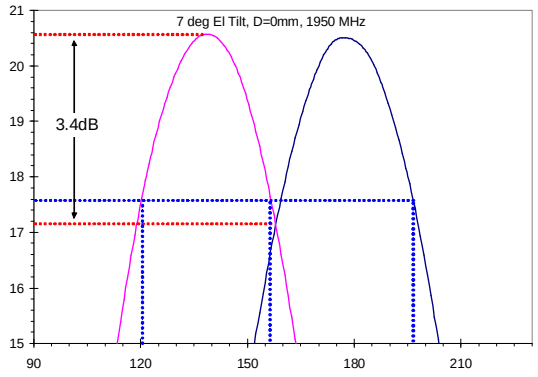

Fig.22(d) Measured cross-over loss (7deg Tilt, D=0mm, 1950MHz)

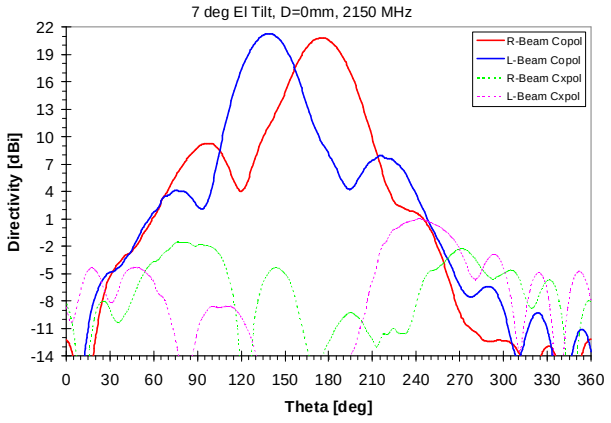

Fig.22(e) Measured DBA Az Pattern (7deg Tilt, D=0mm, 2200MHz)

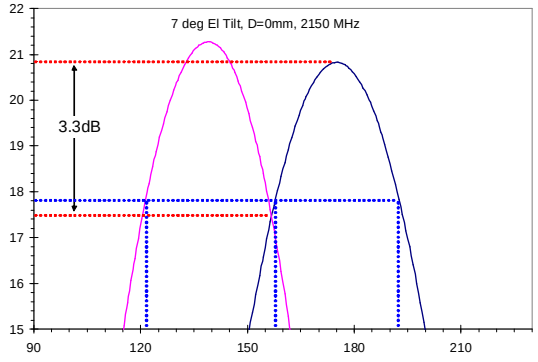

Fig.22(f) Measured cross-over loss (7deg Tilt, D=0mm, 2200MHz)

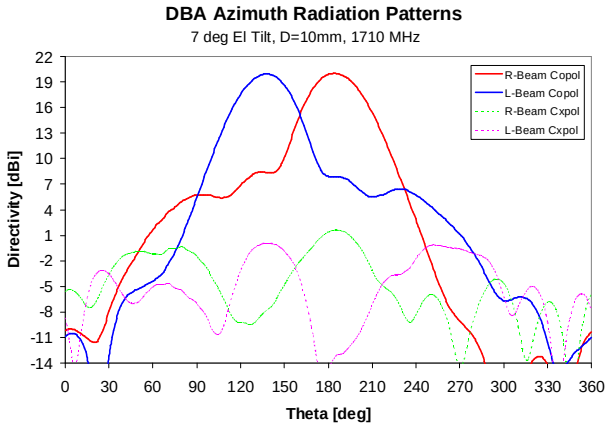

Fig.23(a) Measured DBA Az Pattern (7deg Tilt, D=+10mm, 1710MHz)

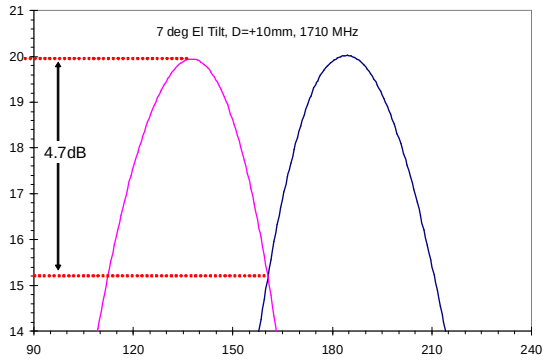

Fig.23(b) Measured cross-over loss (7deg Tilt, D=+10mm, 1710MHz)

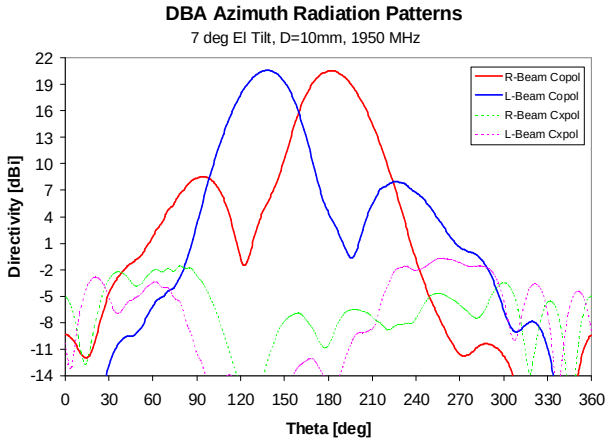

Fig.23(c) Measured DBA Az Pattern (7deg Tilt, D=+10mm, 1950MHz)

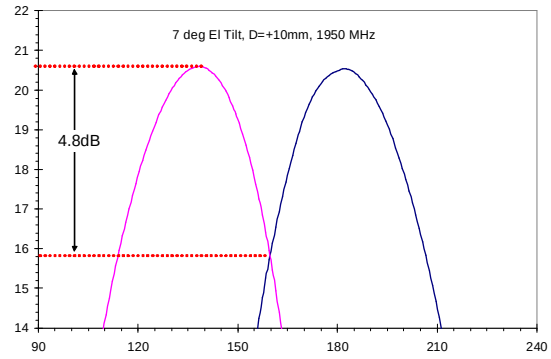

Fig.23(d) Measured cross-over loss (7deg Tilt, D=+10mm, 1950MHz)

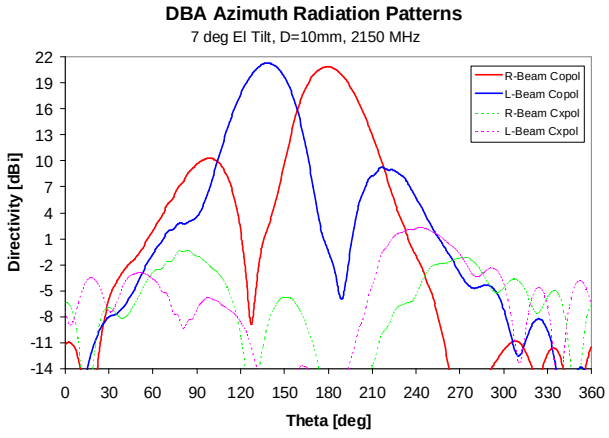

Fig.23(e) Measured DBA Az Pattern (7deg Tilt, D=+10mm, 2200MHz)

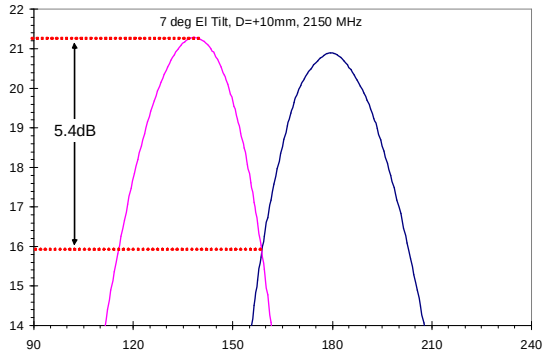

Fig.23(f) Measured cross-over loss (7deg Tilt, D=+10mm, 2200MHz)

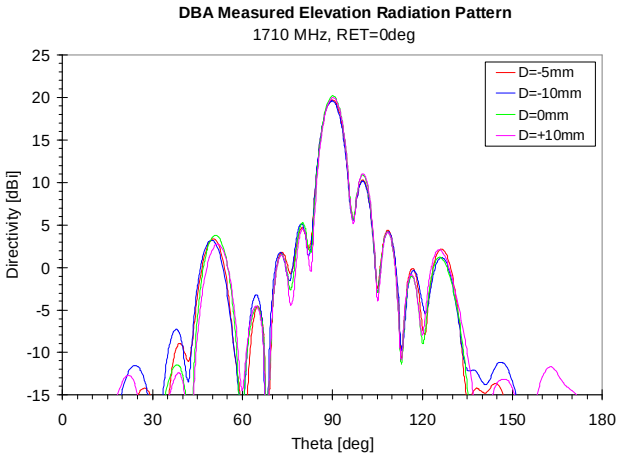

Fig.24(a) Measured DBA EL Pattern (0deg Tilt, 1710MHz)

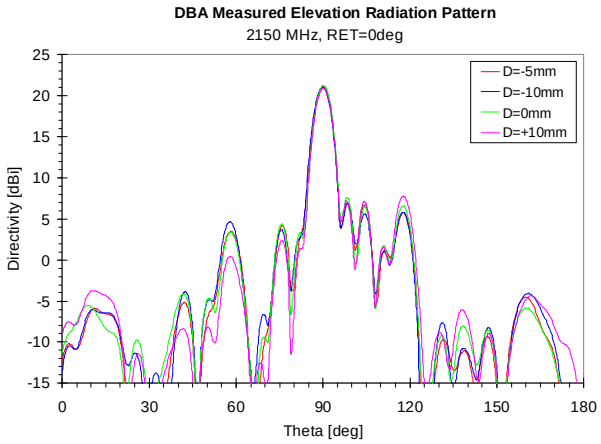

Fig.24(b) Measured DBA EL Pattern (0deg Tilt, 2150MHz)

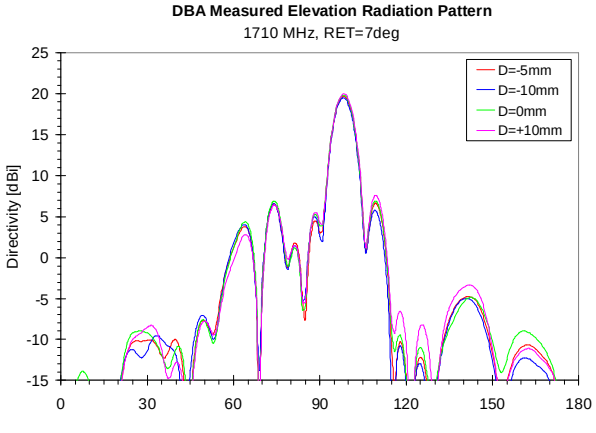

Fig.24(a) Measured DBA EL Pattern (7deg Tilt, 1710MHz)

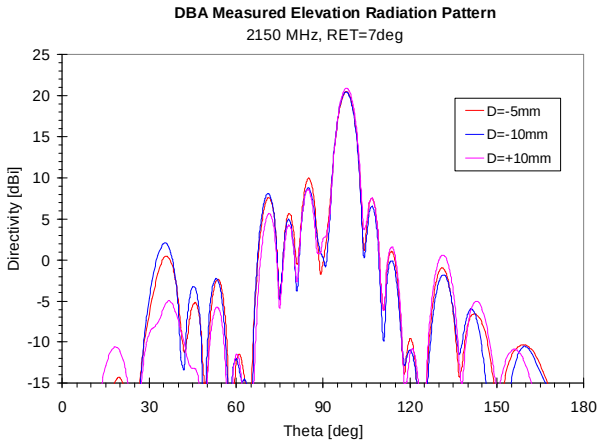

Fig.24(b) Measured EL Pattern (7deg Tilt, 2150MHz)

VIII. DISCUSSION AND RESULTS COMPARISONS

Table 5 summarizes measured antenna parameters of the prototype DBA., including:

1) Cross-over loss
2) Discrimination at peak
3) HPBW
4) Directivity

Table 6 compares these parameters at various values of center displacement, D. HPBW of the two beams are, in general, within 31 deg and 41 deg for D within ±10mm. The measured directivities are approximately between 20 to 21dBi, relatively independent of the displacement D. The cross-over loss varies significantly as the center displacement changes. When D is set to -10mm, the cross-over loss is reduced to -2.3 dB for RET=7deg and -3.5dB when RET=7deg. However, at the same time, the pattern discrimination is also reduced to between 6 to 9dB. The pattern discrimination is improved as the center displacement increases. When D=+10mm, the pattern discrimination is over 13 dB, but the cross-over loss is over 4.7 dB.

The HPBW of the elevation patterns are generally between 6 to 8 deg. A maximum elevation tilt of 7 deg is feasible using the current Powerwave RET phase shifter. Measured elevation patterns at 7deg tilt indicate a slightly higher SLL, above 16dB. Fig. 24 and 25 compare HFSS simulations and measured patterns (1700 MHz and 2200 MHz) in the azimuth plane for D=0.0mm and -5.0mm. These results show very good correlations between the simulations and measured results. However, the HPBW is somewhat better correlated when the displacement D is above 0 mm and the cross-over loss is better predicted when D is below 0mm. Nevertheless, measured patterns and the HFSS simulated results compare relatively well.

Table 5: Summary of measured DBA parameters

Item	Parameter	
1	Frequency	1710 - 2150 MHz
2	Az Beamwidth	Individual : 31 to 41 deg
		Combined : 67 to 92 deg
3	El Beamwidth	6 - 8 deg
4	Directivity	19.7 to 21.3 dBi
5	Cross Pol Level	< -20 dB
5	Polarization	±45 deg
6	El Tilt	6-7 deg (RET)
7	Cross-Over loss	2.3 to 6.5 dB

Table 6: Pattern parameters for various displacement distance D

Distance (D)	Cross-over Loss (dB)	Discrimination At Peak (dB)	HPBW (deg)	Dmax (dBi)
RET=0deg				
D=-10 mm	3.5 - 3.9	>9	32 - 39	19.7 – 21.3
D= 0.0mm	4.9	>12	31 - 37	20.2 – 21.4
D=+10mm	5.9 - 6.5	>16	36 - 41	20.1 – 21.1
RET=7deg				
D=-10 mm	2.3 - 2.8	>6	34 - 40	19.4 – 20.8
D= 0.0mm	3.3 – 3.9	>9	32 - 36	19.7 – 21.3
D=+10mm	4.7 – 5.4	>13	31 - 37	20.0 – 21.3

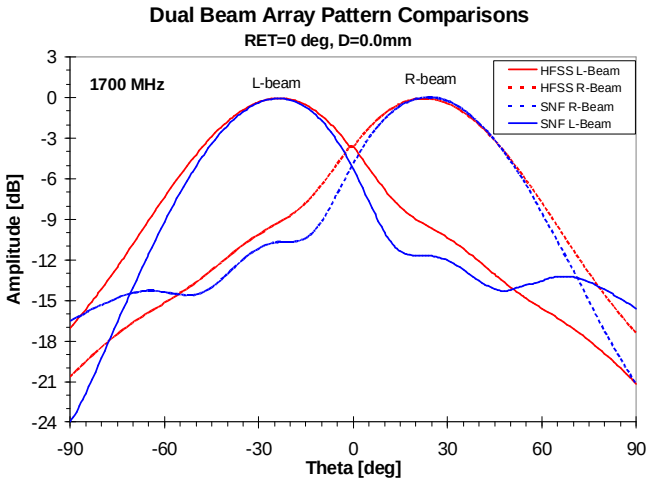

Fig.25(a) Pattern comparison at 1700 MHz, D= 0.0mm

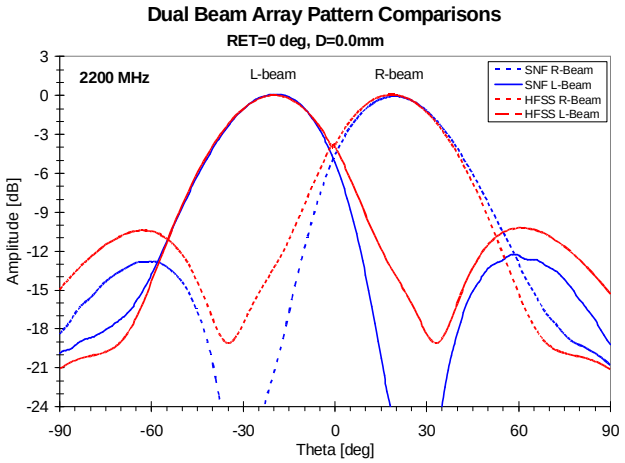

Fig.25 (b) Pattern comparison at 2200MHz, D=0.0mm

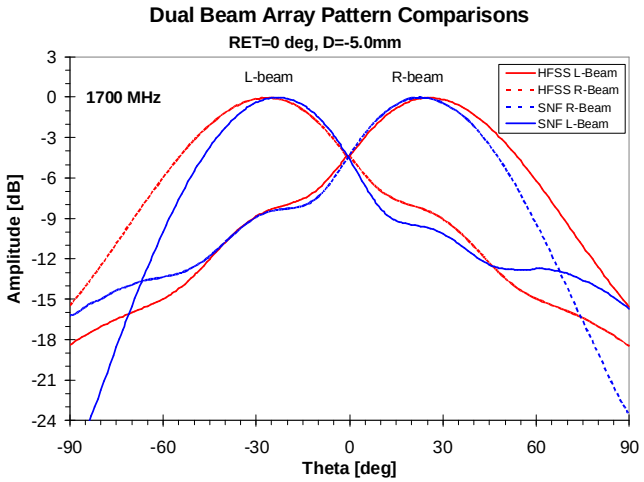

Fig.26(a) Pattern comparison at 1700 MHz, D=-5.0mm

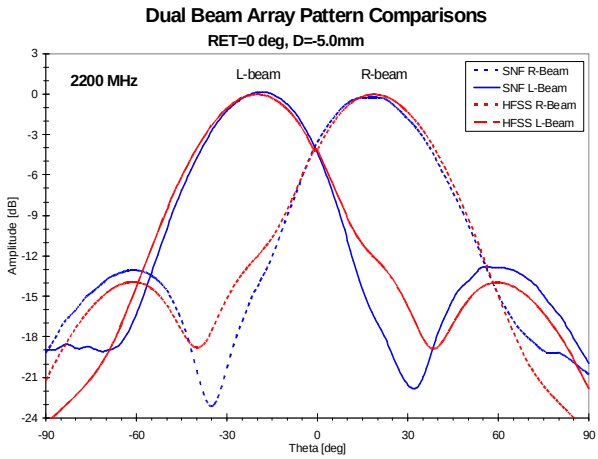

Fig.26(b) Pattern comparison at 2200 MHz, D=-5.0mm

IX. CONCLUSION

Concept of an adjustable dual beam array for cell site enhancement of wireless base station is presented. This method allows for an increase in network capacity through higher order sectorization. The concept is realized using an adjustable three-column array and a compact, low-loss beam former. This structure produces two symmetrical narrow beams with respect to the azimuth boresight within a cellular sector. Radiation patterns of the two beams are adjustable for optimization of coverage of a cellular sector to minimize beam-split loss, or to optimize pattern discrimination and HPBW performance.

The array is capable of delivering more than two beams using a suitable BFN circuit. Theoretically, the device is capable of producing a broad beam for the full azimuth coverage and three narrow beams, simultaneously. It is therefore feasible for the array to transmit signal at one polarization using the broad beam pattern (65 degree), while receive signals at other polarization using the two narrow beams for diversity. For other applications, the dual beam can be used to transmit and to receive simultaneously. The issue with cross-over loss between beams can also be eliminated using three narrow beams, if required. This method allows an effective increase in the overall network capacity as a result of low-loss and narrow beam patterns.

A full array prototype was built and radiation patterns are also presented. The measured results are well correlated with the EM simulated results.

The adjustable DBA and the associated BFN technology under this development are patent pending (Application #12/252,334 and #12/175,725) and are strictly proprietary to Powerwave Technologies.

REFERENCES

[1] S. Foo, B. Vassilakis, “Adjustable dual beam base station antenna,” *Wireless and Mobile Communications, 2008, ICWMC’08, The Fourth International Conference on*, July 27 2008-Aug 01 2008, pp315-320.

[2] R. J. Mailoux, *Phased Array Antenna Handbook*, second edition. Boston, MA: Artech House, 2005.

[3] R. C. Hansen, *Phased Array Antennas*. New York: John Wiley & Sons, 2005.

[4] H. J. Moody, ”The systematic design of the Butler matrix,” *IEEE Trans. On Antennas & Prog.*, vol.12, Issue 6, 1964, pp.786-788.

[5] S. Foo, B. Vassilakis, “Dielectric fortification for wide-beamwidth patch arrays,” *Antennas & Propagation. Society International Symposium 2008, AP-S 2008*, 5-11 July 2008, pp.1-4.